RSC Advances

ROYAL SOCIETY
OF CHEMISTRY

www.rsc.org/advances

Facile protocol for reduction of nitroarenes using magnetically recoverable CoM$_{0.2}$Fe$_{1.8}$O$_4$ (M=Co, Ni, Cu and Zn) ferrite nanocatalysts

Ankita Goyal[a], Surbhi Kapoor[a], Pankaj Samuel[b], Vinod Kumar[c] and Sonal Singhal[a*]

[a]Department of Chemistry, Panjab University, Chandigarh, India-160014.

[b]SAIF, Panjab University, Chandigarh, India-160014.

[c]Icon Analytical Equipment (P) Ltd., Mumbai, 400018, India

[*]sonal1174@gmail.com; sonal@pu.ac.in

CORRESPONDING AUTHOR: Sonal Singhal
Assistant Professor,
Department of Chemistry,
Panjab University,
Chandigarh, India - 160 014
Ph. No. +91-172-2534421(o)
+91-09872118810(m)
Fax No. +91-172-2545074
E-mail: sonal1174@gmail.com

GRAPHICAL ABSTRACT:

Cu ions occupy the catalytically active octahedral sites of the ferrite sub-lattice and present a synergistic effect due to the formation of Cu-Co and Cu-Fe ion pairs which triggers up the catalytic performance of $CoCu_{0.2}Fe_{1.8}O_4$ ferrite nanoparticles for the reduction of nitroarenes.
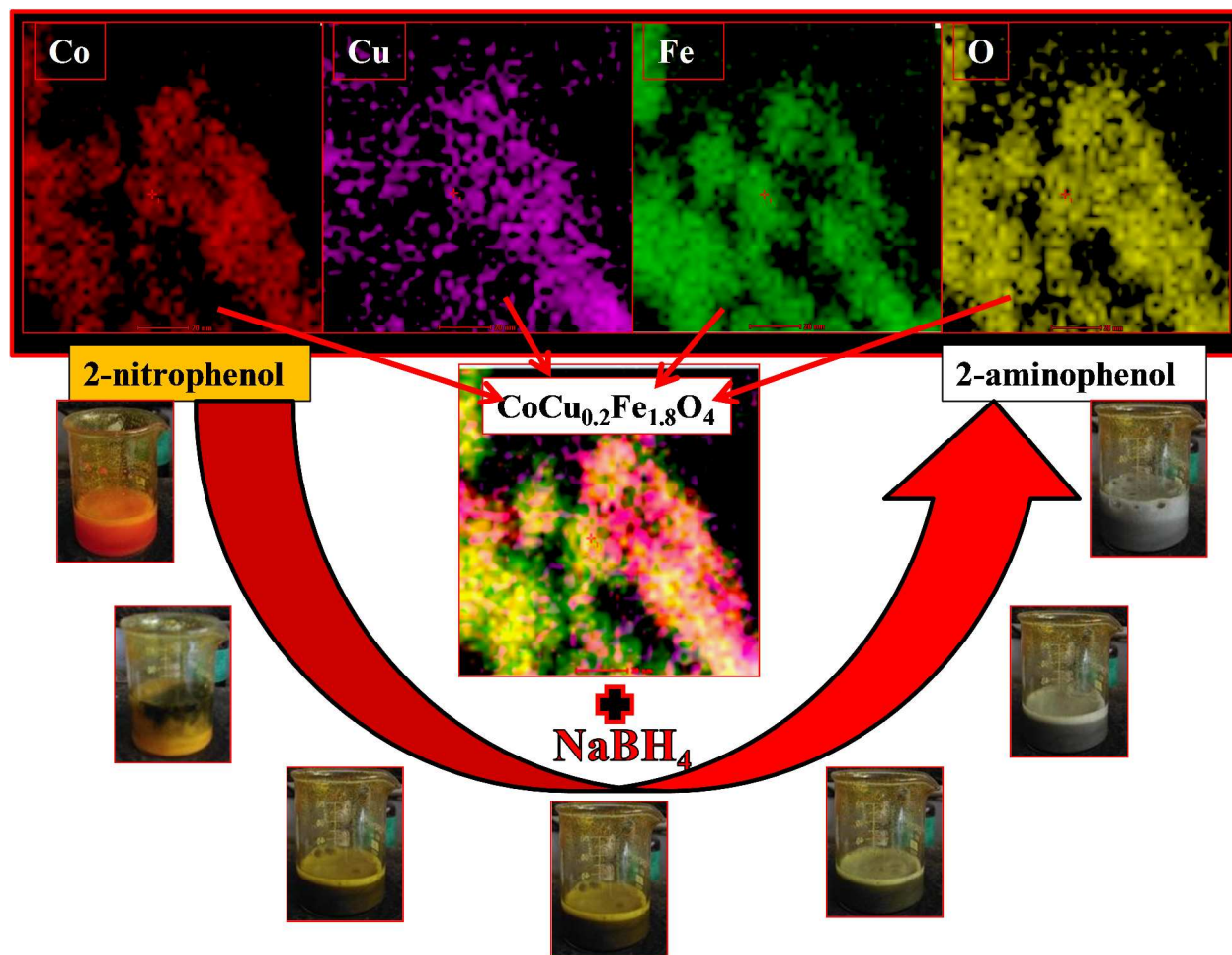
Abstract

Transition metal doped cobalt ferrite ($CoM_{0.2}Fe_{1.8}O_4$ (M= Co, Ni, Cu, Zn)) nanoparticles were fabricated using the sol-gel methodology. The obtained ferrite nanoparticles were annealed at 400 °C and characterized using Fourier transform infra-red spectroscopy (FT-IR), X-ray diffraction (XRD), High resolution transmission electron microscopy (HR-TEM), Vibrating sample magnetometer (VSM) and Energy dispersive X-ray (EDX) and Scanning transmission electron microscopy (STEM). In the FT-IR spectra two bands in the range 1000- 400 cm^{-1} were observed corresponding to the M-O bond in the tetrahedral and octahedral sites. XRD patterns confirmed the formation of cubic spinel structure with Fd-3m space-group. HR-TEM analysis revealed the quasi-spherical shape with particle size in the range 20-30 nm for all the synthesized ferrite nanoparticles. The lattice inter-planar distance of 0.29, 0.25, 0.21 and 0.16 nm obtained from HR-TEM corresponding to (2 2 0), (3 1 1), (4 0 0) and (5 1 1) lattice planes respectively were in complete agreement with the XRD data. The EDX-STEM confirmed the elemental composition as per the desired stoichiometric ratio. The catalytic efficiency of the synthesized ferrite samples was explored for the reduction of nitrophenols. Cu substituted cobalt ferrite nanoparticles ($CoCu_{0.2}Fe_{1.8}O_4$) possessed excellent catalytic activity while $CoM_{0.2}Fe_{1.8}O_4$ (M= Co, Ni and Zn) were inactive for the same. Substrate scope of the developed protocol was also evaluated for the reduction of various CH_3-, NH_2-, Br-, Cl etc. substituted nitroaromatic compounds.

Research highlights:

- $CoM_{0.2}Fe_{1.8}O_4$ (M= Co, Ni, Cu, Zn) fabricated by sol-gel methodology.
- Comparative catalytic efficiency of transition metal doped cobalt ferrites.
- $CoCu_{0.2}Fe_{1.8}O_4$ as excellent catalysts for the reduction of nitroarenes.
- Facile protocol for the synthesis of aromatic amines

Keywords:

Catalytic reduction

Nitroarenes

Magnetically recoverable nanoferrites

Catalytically active octahedral sites

Synergistic effect

1.   Introduction

Aromatic amines are an imperative class of organic compounds which can be served as extremely crucial intermediates and starting materials for the manufacturing of variety of chemicals.[1] The significance of amines in organic chemistry is well recognized as they are an integral part of antipyretic and analgesic drugs, photographic developers, dyeing agents, wood stains, pesticides and herbicides, explosives, surfactants, cosmetics, polymer material auxillaries and corrosion inhibitor in paints.[2]

An effective, facile and widely applicable methodology for the production of aromatic amines is the reduction of nitroaromatic compounds. Conventional reduction methods for the industrial production of aromatic amines are – Bechamp reduction, sulfide reduction and catalytic hydrogenations.[3] Bechamp reduction and sulfide reduction methods are associated with the production of a large amount of sludge, formation of side products, long reaction times and poor selectivity.[4,5] Due to the serious problem of effluent disposal associated with processes, stringent regulatory laws have been implemented in various countries to ban such processes.[6] The use of molecular hydrogen and noble metals is a common route employed in catalytic hydrogenations.[7,8] The other catalytic reduction systems engross sodium borohydride, hydrazine hydrate, formic acid, ammonium formate, and organosilanes in the presence of a metal or its salt which avoids the problem of handling of flammable hydrogen gas.[9,10] Even though the reactions are thermodynamically permissible, catalysts are essential for the reduction to occur. $NaBH_4$ is one such reducing agent which is mild, efficient and very effective for the reduction of nitroaromatic compounds. $NaBH_4$ could hardly reduce nitro groups in the absence of catalysts.[11]

The modern-day nano-sized catalysts have replaced the usual ones because of their skill of providing greater accessibility of active sites for reaction and thereby, enhancing the contact amid the reactants and the catalyst spectacularly.[12] Ferrite nanoparticles have gripped a remarkable consideration for the catalytic applications predominantly in the organic reactions owing to their facile synthetic procedure, thermal and chemical stability, economic viability and outstanding catalytic activity.[13,14] The catalytic activity of the ferrite nanoparticles is mainly associated with the nature and redox potential of the metal ions present on the surface sites, size and surface area of the nanoparticles.[15]

Many research cohorts have synthesized ferrite nanoparticles and their composites and employed them as support for the catalyst and unswervingly as catalysts for the reduction of nitroaromatic compounds. Jang et al. synthesized magnetically separable Rh–Fe$_3$O$_4$ heterodimer nanocrystals and established excellent activities for the selective reduction of nitroarenes and alkenes.[16] Feng et al. discovered that CuFe$_2$O$_4$ magnetic nanoparticles (MNPs) possessed high catalytic performance in the reduction of 4-nitrophenol, with the conversion of 95% within 40 s in the presence of NaBH$_4$ as reducing agent.[17] The Fe$_3$O$_4$@Cu displayed high catalytic activity for the degradation of organic dye. The prepared Fe$_3$O$_4$@Cu exhibited enhanced performance for the reduction of 4-NP as compared to pure Cu nanoparticles.[18] MFe$_2$O$_4$ (M = Ni, Cu, Zn) nanoferrites were employed to catalyze the reductive transformation of nitrophenols to aminophenols in the presence of excess of NaBH$_4$.[19]

Among the spinel ferrites, cobalt ferrite is a hard magnetic material which has been extensively used in various technological applications in the past decades.[20] Cobalt ferrite has a cubic spinel structure with excellent magnetic properties, tunable coercivity, large anisotropy, moderate saturation magnetization, unique light induced coercivity change and chemical stability.[21] Magnetic character of cobalt ferrite allows it to be employed as heterogeneous catalysts in a variety of organic reactions such as C-C, C-N and C-S coupling reactions, oxidation and reduction reactions, decomposition reactions, which can be easily recovered from the reaction mixture using an external magnet.[22-27]

Cobalt ferrite has been found to be inactive for the reduction of nitroarenes.[28] Cobalt ferrite nanoparticles possesses an excellent saturation magnetization which makes them potential magnetically separable catalysts. So to employ cobalt ferrite nanoparticles as catalysts, for the reduction of nitroarenes, attempts have been made in the present investigation by substituting various transition metal ions in to the cobalt ferrite lattice. Various transition metal substituted CoM$_{0.2}$Fe$_{1.8}$O$_4$ (M=Co, Ni, Cu and Zn) cobalt ferrite nanoparticles have been synthesized using sol-gel methodology. This is the first ever report which deals with the comparative catalytic performance of different transition metal doped cobalt ferrite nanoparticles. The swerve in the catalytic efficacy of the highly magnetic cobalt ferrite nanoparticles, with doping of various transition metals (Co, Ni, Cu and Zn) in to its lattice, has been experimented for the reduction of nitrophenols. The scope of the catalytic efficiency of the synthesized ferrite nanoparticles has been established for the reduction of various nitroarenes.

2. Experimental

2.1. Materials and reagents

Ferric nitrate nonahydrate ($Fe(NO_3)_3.9H_2O$, 98%), cobaltous nitrate hexahydrate ($Co(NO_3)_2.6H_2O$, 99.5%), nickel nitrate hexahydrate ($Ni(NO_3)_2.6H_2O$, 98%), cupric nitrate trihydrate ($Cu(NO_3)_2.3H_2O$, 99.5%), zinc nitrate hexahydrate ($Zn(NO_3)_2.6H_2O$, 97.5%), citric acid (99.57%) and sodium borohydride (97%) were obtained from Fisher Scientific. Methanol(99.5%), Ethyl acetate (99.5%), ethylene glycol (99%), hydrochloric acid (37%), and absolute ethanol (99.9%) were supplied by Merck. 2-nitrophenol (98%), 3-nitrophenol (97%), 4-nitrophenol (99%), 1-chloro-2-nitrobenzene (98%), 1-chloro-3-nitrobenzene (98%), 1-chloro-4-nitrobenzene (98%), 1-bromo-2-nitrobenzene (95%), 1-bromo-3-nitrobenzene (95%),1-bromo-4-nitrobenzene (99%), 2-nitrotoluene (98%), 3-nitrotoluene (98%), 4-nitrotoluene (98%), 2-nitroaniline (97%), 3-nitroaniline (96%), 4-nitroaniline (98%), 1,4-dichloro-2-nitrobenzene (99%), 2,4-dichloro-1-nitrobenzene (99%), 2-chloro-4-nitroaniline (99%), 4-chloro-2-nitroaniline (98%), 2,6-dichloro-4-nitroaniline (96%), 2,4-dibromo-1-nitrobenzene (95%), 2,5-dibromo-1-nitrobenzene (99%) and 2,6-dibromo-4-nitroaniline (95%) were supplied by Avra Synthesis. All the chemicals were of analytical grade and were used as such. Distilled water was obtained using an ultra filtration system (Milli-Q, Millipore)

2.2. Fabrication of $CoM_{0.2}Fe_{1.8}O_4$ (M=Co, Ni, Cu and Zn) catalyst

$CoM_{0.2}Fe_{1.8}O_4$ (M=Co, Ni, Cu and Zn) ferrite compositions were synthesized using sol-gel methodology.[29] In a characteristic synthesis stoichiometric amounts of the required metal salts and citric acid (in the ratio 1:1 to precursor metal salts) were taken and dissolved separately in minimum amount (5-10 mL) of distilled water with stirring and heating at ~ 60 °C. The clear salt solutions were then mixed, heated at 60-70 °C and subjected to magnetic stirring followed by the addition of citric acid solution. The stirring and heating of the solution was continued and 10 mL of ethylene glycol was added to promote gelation of the solution. The acquired solution was heated to 80- 90 °C for ~ 2 hours till gels were formed. The obtained gels were further ignited in the self-propagation manner to obtain ferrite powders. The acquired ferrite nanoparticles were annealed at 400 °C for 2 hours in a muffle furnace.

2.3. Physical measurements

The synthesized ferrite samples were characterized using powder X-ray diffraction technique. Panalytical's X'Pert Pro diffractometer equipped with vertical theta-theta goniometer

and x'Celerator solid-state detector. The conformation of the formation of M-O bonds in the octahedral and the tetrahedral sites of the ferrite sub-lattice was carried out using FT-IR spectroscopy employing Perkin Elmer - Spectrum RX-IFTIR instrument with the resolution of 1 cm^{-1} and scan range of 4000 cm^{-1} to 400 cm^{-1}. Shape, size and elemental composition of the synthesized nanocatalyst were examined using High Resolution Transmission Electron Microscopy (HR-TEM) and Energy dispersive X-ray spectroscopy (EDS). For the HR-TEM, EDS and STEM analysis FEI Tecnai (G2 F20) operating at 200 keV was used. Energy dispersive X-ray spectroscopy (EDS) was performed using an adjacent EDAX Inc system. The metal contents were calculated by EDS quantification. Magnetic measurements were carried out using Vibrating sample magnetometer (VSM) (155, PAR) in the magnetic field range of -10,000 Oe to 10,000 Oe at room temperature. The selective formation of nitrophenols and its reaction kinetics was studied by UV-Visible spectrophotometer (JASCO model V-530). The derived products were analyzed and confirmed by using THERMO GC (TRACE 1300) with a Thermo TG 5MS 5% phenyl Methylpolysiloxane capillary column (30m X 0.25mm X 0.25μm)) and a triple quadrupole Thermo MS (TSQ 8000) mass spectrometer. Helium was used as carrier gas at a constant flow-rate of 1.1 $mLmin^{-1}$ and the desorption temperature in the injector was 250 °C. Temperature conditions used for the separation were as follows: initial temperature was 70 °C (hold for 2 minutes), followed by increase at 10 °C/min to 240 °C, and finally at 5 °C/min to 270 °C (hold for 10 minutes) and total analysis time was of 35 minutes.

2.4. Catalytic procedure and spectrophotometric determination for the reduction of nitrophenols

To investigate the catalytic reduction of nitrophenols, 20 mL of 0.036 mol L^{-1} aqueous solution of nitrophenol was taken in a 100 mL beaker and 50 equivalents of $NaBH_4$ was added. The solution was subjected to constant stirring. With the addition of $NaBH_4$, the colour of the solution darkened due to the formation of phenolate ion. After 1 minute desired amount of nano ferrite catalyst was added and stirring was continued at room temperature. The dark yellow color of the solution gradually vanished, signifying the reduction of nitrophenol. The reaction progress was checked by drawing 30 μL of the reaction mixture at regular time intervals and quenching it by adding 5 mL of 2 M HCl. The conversion of nitrophenol to aminophenol was checked by UV-Visible spectroscopy by measuring the absorption maxima corresponding to reactant nitrophenol and product aminophenol.

2.5. Reduction of nitroarenes

For the reduction of other nitroarenes compounds methanol was used as solvent due to insolubility of the reagents in aqueous medium. In a typical reduction reaction, 0.05 g of the nitroarene derivative was dissolved in 20 mL of methanol, 50 equivalent of $NaBH_4$ was added and the solution was subjected to magnetic stirring. The stirring was continued, after 1 minute the catalyst was added and the reaction started at once with the addition of catalyst. The progress of the reaction was checked using GC analysis. After the completion of reaction the catalyst was separated magnetically and the solvent was evaporated using rota-evaporator and to the obtained solid, water and ethyl acetate was added. The ethyl acetate extract was separated and dried using Na_2SO_4. The structure elucidation of the product obtained was confirmed using GC-MS. The separated catalyst was washed with water and acetone repeatedly to remove the organic and inorganic part and dried for further use.

3. Results and discussion

3.1. Fourier transform infra-red (FT-IR) spectroscopy

FT-IR spectra were recorded for all the synthesized ferrite nanoparticles to confirm the formation of M-O bond.[30] Ferrites generally exhibit two peaks corresponding to the M-O bonds made by the metal ions present in the octahedral and the tetrahedral sites of the oxide ion lattice. Two infra-red frequency bands, in the range of 600-400 cm^{-1} were observed for all the ferrite compositions.[31] Lower frequency band at ~ 415 cm^{-1} is assigned to the stretching mode of the M-O bond in the octahedral site and higher frequency band at ~560 cm^{-1} is attributed to the stretching vibrations of the M-O clusters in the tetrahedral site.[32] The FT-IR spectra for $CoM_{0.2}Fe_{1.8}O_4$ (M=Co, Ni, Cu and Zn) ferrite nanoparticles (annealed at 400 °C) are shown in Fig. 1.

3.2. Powder X-ray Diffraction (XRD) studies

Powder X-ray diffraction patterns were recorded for the entire synthesized ferrite compositions. Fig. 2 (a) shows the XRD patterns of $CoM_{0.2}Fe_{1.8}O_4$ (M=Co, Ni, Cu and Zn) ferrite nanoparticles annealed at 400 °C. The peaks appearing at 2θ (relative intensity) values of 30.272° (40), 35.743° (100), 37.280° (5), 43.472° (15), 53.886° (8), 57.186° (45), 62.726° (65), 71.401° (3), 73.995° (13), 79.867° (3) and 86.909° (5) could be assigned for the X-ray scattering from (2 2 0), (3 1 1), (222), (4 0 0), (4 2 2), (5 1 1), (4 4 0), (6 2 0), (5 3 3), (4 4 4) and (6 4 2) planes of the spinel crystal lattice (JCPDS card no. 00-001-1121).[33] Indexing of the peaks with

their respective lattice planes of the cubic unit cell affirmed the formation of single phase with Fd-3m space group. An enlarged (311) peak for all the XRD patterns corresponding to $CoM_{0.2}Fe_{1.8}O_4$ (M=Co, Ni, Cu and Zn)) nanoferrites respectively is shown in Fig. 2(b). A slight shift in the peak towards higher 2θ values from Co to Cu was observed which could be due to decreasing trend of ionic size from Co to Cu. Peak corresponding to Zn doped cobalt ferrite somewhat shifted towards left due to larger ionic size of zinc. Similar shift in the 2θ values with the substitution of smaller sized Mg^{2+} ions in to the cobalt ferrite lattice was observed by Bhukal et al.[34] Crystallite size was calculated from the line broadening of the most intense (3 1 1) peak using the classical Scherrer equation.[35,36] The crystallite sizes for all the ferrite nanoparticles were found to be in the range of 14 - 18 nm. The lattice parameter values were evaluated using the Le bail refinement method. The values of lattice parameter were observed to be in the range of 8.37-8.39 A°. The values of crystallite size, lattice parameters and X-ray densities are given in Table. 1.

3.3   Morphological characterization

For the assessment of size, shape, crystallinity and elemental analysis HR-TEM (High resolution transmission electron microscopy), EDX (Energy dispersive X-ray) and EDX-STEM (Energy dispersive X-ray- Scanning transmission electron microscopy) studies were carried out. The Low resolution TEM images for $CoM_xFe_{2-x}O_4$ (x= 0.2, M=Co, Ni, Cu and Zn) ferrite nanoparticles shown in Fig. 3(a), Fig. 4(a), Fig. 5(a) and Fig. 6(a) revealed the quasi-spherical shape for all the synthesized samples. The size of the particles for the all the ferrite samples was observed to be in the range of 20- 30 nm. The HR-TEM images (Fig. 3(b), Fig. 4(b), Fig. 5(b) and Fig. 6(b)) for $CoM_{0.2}Fe_{1.8}O_4$ (M=Co, Ni, Cu and Zn) ferrite nanoparticles showed the lattice inter-planar distance of 0.29, 0.25, 0.21 and 0.16 nm which corresponded to (2 2 0), (3 1 1), (4 0 0) and (5 1 1) lattice planes respectively.[37] Lattice interplanar distance is not clearly visible in Fig. 4(b) so magnified images of the selected portion of the image are shown in Fig. S1 (supporting file). Xin et al. carried out the detailed studies related to the lattice interplanar distance of nanoparticles.[38] The lattice inter-planar distance values provided by the HR-TEM were in full agreement with the data provided by XRD analysis.

The SAED (Selected area electron diffraction) patterns for $CoM_xFe_{2-x}O_4$ (x= 0.2, M=Co, Ni, Cu and Zn) ferrite nanoparticles are shown in Fig. 3(c), Fig. 4(c), Fig. 5(c) and Fig. 6(c) respectively. In SAED pattern, each spot of SAED forms a disk of radii in few hundreds of

nanometer. SAED patterns of a crystalline sample are good enough to attain the symmetry of its lattice and to calculate its inter-planar distances using the Bragg's law. A single phase nano-crystalline material is made up of many tiny single crystals whose diffraction patterns appears to be a superposition of single crystal spot patterns i.e. a series of concentric rings resulting from many spots very close together at various rotations around the central beam spot. Each ring is a reflection of the family of planes with different inter-planar spacing.[39] The planes corresponding to the obtained concentric rings are marked in the given SAED patterns which were observed to be in full concurrence with the XRD data.

The STEM images for $CoM_{0.2}Fe_{1.8}O_4$ (M=Co, Ni, Cu and Zn) ferrite nanoparticles are shown in Fig. 3(d), Fig. 4(d), Fig. 5(d) and Fig. 6(d) respectively. The EDX spectra for $CoM_{0.2}Fe_{1.8}O_4$ (M=Co, Ni, Cu and Zn) ferrite nanoparticles (Fig. 3(e), Fig. 4(e), Fig. 5(e) and Fig. 6(e)) confirmed the qualitative as well as the quantitative elemental composition to be as per the set stoichiometric ratio. The additional unavoidable signals corresponding to Cu and C were due to carbon coated copper grid.[40] Furthermore a typical enlarged version of EDX pattern shown in Fig. 4 (e) with all the marked signals and corresponding K and L shells of the elements present in the sample is given as Fig. S2 in the supporting file. The typical STEM-EDX mapping with the atomic distribution of the elements for $CoCu_{0.2}Fe_{1.8}O_4$ is shown in Fig. 7, which evidenced the homogeneous distribution of different elements in the synthesized ferrite nanoparticles.[41] Only the presence of the four elements i.e. Co, Cu, Fe and O confirmed the purity of the sample.

3.4. Magnetic measurements

The room temperature hysteresis loops for the $CoM_{0.2}Fe_{1.8}O_4$ (M=Co, Ni, Cu and Zn) ferrite nanocatalysts as obtained and annealed at 400 °C were recorded using the Vibrating Sample magnetometer (VSM) (Fig. 8). For the as obtained samples the hysteresis was not observed, owing to amorphous nature. The room temperature hysteresis loops for the samples before annealing were also reported by Ferrer et al.[42] The values of saturation magnetization (M_s), remanence (M_r), coercivity (H_c) and squareness (S) for all the samples annealed at 400 °C are given in Table. 1. The saturation magnetization values were observed to be in the range of 36-40 emu/g and were found to be less than the saturation magnetization of bulk counterparts.[43] This could be attributed to the reason that the extent of magnetization of a magnetic particle in an external field is proportional to its size value.[44] Sharma et al. reported the saturation

magnetization of cobalt ferrite nanoparticles annealed at 400 °C to be 65 emu/g.[45] With the replacement of 10 % of Fe ions in the octahedral sites a decrease in saturation magnetization of $CoM_{0.2}Fe_{1.8}O_4$ (M=Co, Ni, Cu and Zn) ferrite nanocatalysts was observed. This decrease in the values of saturation magnetization with the introduction of different dopant metals could be related to the distribution of cations among the octahedral and the tetrahedral sites of the ferrite sub-lattice. Saturation magnetization is directly proportional to the magnetic moment per formula unit and magnetic moment further depends upon the number of unpaired electrons present in the cations located in the respective sites.[46] According to Neel's two sub-lattice model, the magnetic moment per formula unit in Bohr magneton $n_B^N(\chi)$ is expressed as:

$$n_B^N(\chi) = M_B(\chi) - M_A(\chi)$$

where, M_B and M_A are magnetization of B and A sub-lattices, respectively. When M= Co^{3+} (3 unpaired electrons) Ni^{2+} (2 unpaired electrons) and Cu^{2+} (1 unpaired electrons) replaces Fe^{3+} (5 unpaired electrons) decrease in the magnetization of the octahedral site is there, which further decreased the overall magnetization. This established the octahedral site occupancy of the substituent metal ions (Co, Ni and Cu). Zn^{2+} (no unpaired electron) have site preference for tetrahedral site. So saturation magnetization should have increased, but it decreased. This behavior could be explained on the basis that exchange interactions between A and B sites got lowered. With Zn^{2+} having diamagnetic character, only mutual interaction between the ions on B sites was possible. This resulted in strengthening of B-B interaction and weakening of A-B interaction.[47,48] The coercivity value was comparatively low for Cu substituted cobalt ferrite nanoparticles annealed at 400 °C, this could be due to the decrease in magneto crystalline anisotropy as observed by An et al.[49] The squareness (S) was calculated according to the equation- $S=M_r/M_s$.[50]

3.5.   Catalytic property evaluation

3.5.1. Reduction of nitrophenols

For the assessment of the comparative catalytic activity of the synthesized ferrite nanoparticles reduction of nitrophenols was performed. The reduction reaction was carried out in the presence of 50 equivalents of sodium borohydride as reducing agent. The reduction reaction could not be carried out without the catalyst because sodium borohydride has less ability to reduce nitrobenzene without other additives. But $NaBH_4$ was crucial for the same. Reduction of nitrophenols presents a visible color change as an indication of the complete conversion of the

reactant nitrophenols to the corresponding aminophenols.[51] So the reduction of nitrophenols was chosen to study the kinetics.

3.5.1.1. Catalytic efficacy of CoM$_{0.2}$Fe$_{1.8}$O$_4$ (M=Co, Ni, Cu and Zn)

Catalytic activity of the synthesized CoM$_{0.2}$Fe$_{1.8}$O$_4$ (M=Co, Ni, Cu and Zn) were evaluated by performing the reduction of 4-nitrophenol. Reduction was performed in the presence of 50 equivalents of NaBH$_4$ (reducing agent) and varying amounts (2, 5, 10, 20 and 30 mole %) of CoM$_{0.2}$Fe$_{1.8}$O$_4$ (M=Co, Ni, Cu and Zn) ferrite nanoparticles as catalyst. Co, Ni and Zn substituted cobalt ferrite nanoparticles were observed to be inactive for the reduction of nitrophenols even when 30 mole % catalysts were used. CoCu$_{0.2}$Fe$_{1.8}$O$_4$ ferrite nanoparticles were found to be active for the same and with 30 mole % of catalyst the reduction of 4-nitrophenol was accomplished in 1.5 minutes. This behavior could be explained on the basis of site preference, nature of the doped metal ion and synergistic behavior of the ions present in the catalytically active surface octahedral sites. In cobalt ferrite both Co and Fe ions are present in the octahedral sites and cobalt ferrite itself is inactive for the reduction of nitrophenols.[41] With the doping of 10 % of Cu, cobalt ferrite nanoparticles got activated for the reduction of nitrophenols and no improvement in catalytic activity was observed with doping of Co, Ni and Zn ions. Cu ions occupy the catalytically active octahedral sites of the ferrite sub-lattice and present a synergistic effect due to the formation of Cu-Co and Cu-Fe ion pairs which triggers up the catalytic performance of CoCu$_{0.2}$Fe$_{1.8}$O$_4$ ferrite nanoparticles for the reduction of nitroarenes.[52-54]

3.5.1.2. UV-Visible spectroscopy

The progress of the reduction of nitrophenols can be easily monitored using UV-Visible spectroscopy. In the UV-Visible spectrum the Absorption maxima corresponding to the 2-, 3- and 4- nitrophenol appears at 350, 325 and 317 nm respectively. With the progress of the reaction the yellow color of the nitrophenols start to fade and corresponding absorption maxima start demolishing. New peaks corresponding to the 2-, 3- and 4-aminophenol emerge at 267, 269 and 268 nm respectively.[55,56] The effect of catalyst loading was explored and it was observed that with increase in the amount of catalyst the reaction became faster. Improvement in the catalytic activity could be due to increase in the number of catalytic sites with increase in the amount of catalyst. More the number of catalytic sites faster will be the reaction and lesser will be the completion time. The values of completion time are given in Table. 2. With increase in the

amount of catalyst from 2 mole % to 30 mole % the value of completion time for the reduction of 2-nitrophenol decreased from 8 minutes to 1 minute. With further increase in the catalyst amount the completion time remain constant i.e no further improvement was observed. The effect of catalyst loading typically for the reduction of 2- nitrophenol when catalyst amount was varied from 2 mole % to 100 mole % is shown in Fig. S3 (supporting file). Typical UV-Visible spectra for the reduction of 2-, 3- and 4- nitrophenol in the presence of 10 mole % $CoCu_{0.2}Fe_{1.8}O_4$ ferrite nanoparticles as catalyst are shown in Fig. 9. The graphs of absorbance vs. time and % conversion vs. time for the reduction of nitrophenols in the presence of varying amounts of catalyst (2, 5, 10, 20 and 30 mole %) are shown in Fig. 10 and Fig. 11 respectively.

3.5.1.3. Chemical Kinetics

Reduction of nitrophenols was carried out in the presence of excess of sodium borohydride. So, the concentration of sodium borohydride could be considered to be constant during the reaction and the reduction follows pseudo first order kinetics with respect to the concentration of the reactant nitrophenol.[57] The apparent rate constant (k_{app}) for the pseudo first order reaction could be defined through the equation:

$$\ln \frac{C_t}{C_0} = -k_{app}t$$

The absorbance of nitrophenols in UV-Visible spectra is proportional to its concentration in the reaction medium, the ratio of absorbance at any time t (A_t) to that at time t=0 (A_0) is proportional to the ratio of concentration at any time t (C_t) to that at time t=0 (C_0). So the apparent first order rate law equation could be written as[58]:

$$ln \frac{A_t}{A_0} = -k_{app}t$$

The plots of $\ln(A_t/A_o)$ vs time (t) for the reduction of 2-, 3- and 4-nitrophenol in the presence of varying amount (2 mole%, 5 mole%, 10 mole%, 20 mole%, 30 mole%) of $CoCu_{0.2}Fe_{1.8}O_4$ catalyst are shown in Fig. 12. The values of apparent rate constants obtained from the slope of the plot of $\ln(A_t/A_o)$ vs time (t) are given in Table 3. The rate constant values for the reduction of nitrophenols in the presence of $CoCu_{0.2}Fe_{1.8}O_4$ ferrite nanoparticles as catalyst were observed to be higher in comparison with pure $CuFe_2O_4$ and $CoFe_2O_4$ nanoparticles reported in our previous publications.[19,28] Furthermore, $CoCu_{0.2}Fe_{1.8}O_4$ ferrite nanoparticles as catalyst were observed to possess better catalytic activities in contrast with other catalysts reported in literature.[56,59]

3.5.2. Substrate scope

To evaluate the substrate scope of the synthesized $CoCu_{0.2}Fe_{1.8}O_4$ ferrite nanoparticles, reduction of various chloro, bromo, methyl, dichloro, dibromo and amino substituted nitroaromatic compounds was carried out. 10 mole % of the catalytic amount was chosen for the reduction of nitroarenes so to study the completion times and conversions effectively. Most of nitroarenes could be reduced to corresponding aromatic amines with excellent conversions and selectivity in the present protocol. It was found to be highly efficient and selective for the reduction of chloro, methyl, dichloro and amino substituted nitroaromatic compounds. However, the bromo substituted nitroaromatic compounds presented relatively low yields because of facile dehalogenation of such compounds in current reaction condition. TOF (turn over frequency) was calculated as moles of product generated per moles of catalyst used in the given time. The completion time, percent conversion and percent product selectivity deduced from the GC-MS analysis and calculated TOF's for the reduction of all the nitroarene derivatives are given in Table. 4.

3.5.3. Probable mechanistic pathway

Catalytic activity of the ferrite nanoparticles is critically related to metal ions present on the surface exposed octahedral sites of the sublattice formed by oxygen ions. In addition the size of the particles, shape of the particles, redox properties of metal ions and the cation distribution also affects the catalytic activity of the ferrite nanoparticles.[60] In the present protocol, $NaBH_4$ dissolves and ionizes in the solvent with the generation of borohydride ions. When the catalyst is added, borohydride ions get diffused towards the surface of the catalyst and lead to the formation of metal-hydride (M-H) complex.[61] Nitroarenes also get adsorbed onto the catalyst surface with reversible adsorption and desorption. Thereafter, hydride ions get transferred from the M-H complex to nitroarenes compounds both present at the surface of the catalyst. Ion pairs present in the surface exposed octahedral sites play the lead role in the transfer of hydride ions. Thereby reduction of nitro derivative to the corresponding amine derivative is accomplished followed by desorption of the product formed.

3.5.4. Reusability of the catalyst

Reusability of the $CoCu_{0.2}Fe_{1.8}O_4$ ferrite nanoparticles was established by carrying out catalytic reduction of 4-nitrophenol using the recycled catalyst. The $CoCu_{0.2}Fe_{1.8}O_4$ ferrite nanoparticles were sufficiently magnetic so could be separated out of the reaction mixture using

an external magnet after the completion of the catalytic reaction. The reaction mixture was decanted keeping the catalyst stuck on the wall of the beaker using an external magnet. The recovered catalyst was washed repeatedly with methanol and distilled water and dried. The dried catalyst was used for the next catalytic run. The reduction was performed, using the same catalyst with no considerable change in the catalytic activity in terms of conversion percentage and completion time, up to six catalytic run. For the next catalytic reaction small increase in the completion time was observed, due to the loss of catalyst. The variation of completion time for the successive catalytic runs is shown in Fig. 13.

4.   Conclusions

Transition metal doped cobalt ferrite $CoM_{0.2}Fe_{1.8}O_4$ (M=Co, Ni, Cu and Zn) nanoparticles with quasi-spherical shape has been successfully fabricated using sol-gel methodology. The formation of pure phase, successful incorporation of the doped metal in to the cobalt ferrite lattice, elemental composition and homogeneous distribution of the metal cations has been confirmed using XRD and EDX-STEM analysis. The effect of various transition metal cations on to the catalytic activity of the cobalt ferrite nanoparticles has been explored for the reduction of nitroarenes. $CoM_{0.2}Fe_{1.8}O_4$ (M=Co, Ni and Zn) ferrite nanoparticles have been observed to be inactive for the reduction of nitrophenols while $CoCu_{0.2}Fe_{1.8}O_4$ ferrite nanoparticles have been established to be excellent catalysts for the same. Catalytic activity of Cu doped cobalt ferrite nanoparticles is related to the octahedral site preference of Cu ions. The addition of the Cu ions in to the catalytically active octahedral sites of the ferrite sub-lattice present a synergistic effect due to the formation of Cu-Co and Cu-Fe ion pairs which triggers up the catalytic performance of $CoCu_{0.2}Fe_{1.8}O_4$ ferrite nanoparticles. Cu doped cobalt ferrite nanoparticles can be readily prepared from available starting materials and have been recognized as a reusable catalyst having very good stability to air, moisture and elevated temperatures. The proposed protocol applied here for the reduction of nitroarenes lead to better yields in approximately shorter times compared with previous reports using other catalytic systems. Therefore, considering these and their compliance with Green Chemistry principles, this methodology is a useful and general method for the synthesis of aromatic amines. In addition, because of the total recovery of the metal-based catalyst from the reaction media, the procedure can be applied in pharmaceutical and other sensitive synthetic procedures.

Acknowledgements

References:

1. Y. S. Feng, J. J. Ma, Y. M. Kang and H. J. Xu, *Tetrahedron.*, 2014, 70, 6100-6105.

2. M. Tumma and R. Srivastava, *Catal. Commun.*, 2013, 37, 64–68.

3. X. Liu, H. Cheng and P. Cui, *Appl. Surf. Sci.,* 2014, 292, 695– 701.

4. F. Cardenas-Lizana, X. Wang, D. Lamey, M. Li, M. A. Keane and L. Kiwi-Minsker, *Chem. Eng. J.,* 2014, 255, 695–704.

5. S. K. Maity, N. C. Pradhan and A. V. Patwardhan, *Appl. Catal., A*, 2006, 301, 251–258.

6. A. S. Kulkarni and R. V. Jayaram, *Appl. Catal., A*, 2003, 252, 225–230.

7. P. K. Santra and P. Sagar, *J. Mol. Catal. A: Chem.*, 2003, 197, 37–50.

8. M. L. Kantam, T. Bandyopadhyay, A. Rahman, N. M. Reddy and B. M. Choudary, *J. Mol. Catal. A: Chem.*, 2003, 197, 37–50.

9. Y. Feng, A. Wang, H. Yin, X. Yan and L. Shen, *Chem. Eng. J.*, 2015, 262, 427–435.

10. S.K. Ghosh, M. Mandal, S. Kundu, S. Nath and T. Pal, *Appl. Catal., A*, 2004, 268, 61–66.

11. S. P. Jr., D. M. Cedillo, C. Tamez, N. Izquierdo, J. G. Parsons and J. J. Gutierrez, *Tetrahedron Lett.,* 2014, 55, 5468–5470.

12. P. L. Gai, R. Roper and M. G. White, *Solid State Mater. Sci.***,** 2002, 6, 401–406.

13. F. M. Moghaddam, G. Tavakoli and H. R. Rezvani, *Catal. Commun.*, 2015, 60, 82–87.

14. C. Liu, J. Ma and H. Chen, *RSC adv.,*2012, 2, 1009-1013.

15. S. Jauhar and S. Singhal, *Ceram. Int.*, 2014, 40, 11845–11855.

16. Y. Jang, S. Kim, S. W. Jun, B. H. Kim, S. Hwang, I. K. Song, B. M. Kim and T. Hyeon. *Chem. Commun.*, 2011, 47, 3601–3603.

17. J. Feng, L. Sua, Y. Maa, C. Ren, Q. Guo and X. Chen, *Chem. Eng. J.*, 2013, 221, 16–24.

18. M. Tang, S. Zhang, X. Li, X. Pang and H. Qiu, *Mater. Chem. Phys.*, 2014, 148, 639-647.

19. A. Goyal, S. Bansal and S. Singhal, *Int. J. Hydrogen Energy*, 2014, 39, 4895-4908.

20. R. Ianos, *Mater. Lett.,* 2014, 135, 24–26.

21. K. K. Mohaideen and P. A. Joy, *J. Magn. Magn. Mater.*, 2013, 346, 96–102.

22. R. Dumitru, F. Papa, I. Balint, D. C. Culita, C. Munteanu, N. Stanica, A. Ianculescu, L. Diamandescu and O. Carp, *Appl. Catal., A*, 2013, 467, 178–186.

23. M. Kooti and M. Afshari, *Sci. Iran. F*, 2012, 19(6), 1991–1995.

24. K. K. Senapati, S. Roy, C. Borgohain and P. Phukan, *J. Mol. Catal. A: Chem.*, 2012, 352, 128– 134.

25. I. Genova, T. Tsoncheva, M. Dimitrov, D. Paneva, B. Tsyntsarski, R. Ivanova, Z. Cherkezova-Zheleva, T. Budinova, D. Kovacheva, I. Mitov and N. Petrov, *Catal. Commun.*, 2014, 55, 43–48.

26. S. Akbayrak, M. Kaya, M. Volkan and S. Özkar, *J. Mol. Catal. A: Chem.*, 2014, 394, 253–261.

27. Y. Hammiche-Bellal, A. Benadda, L. Meddour-Boukhobza, S. Barama, A. Djadoun and A. Barama, Catal. Commun., 2013, 42, 62–67.

28. A. Goyal, S. Bansal, V. Kumar, J. Singh and S. Singhal, *Appl. Surf. Sci.*, 2015, 324, 877–889.

29. R. Sharma and S. Singhal, *Physica B*, 2013, 414, 83–90 .

30. B. Gillot, J. Lorimier, F. Bernard, V. Nivoix, S. Douard and Ph. Tailhades, *Mater. Chem. Phys.*, 1999, 61, 199-206.

31. M. Hashima, A. S. Kumar, S. E. Shirsath, R. K. Kotnala, J. Shah and R. Kumar, *Ceram. Int.*, 2013, 39, 1807–1819.

32. M. A. Gabal, Y. M. Al Angari, A. Y. Obaid and A. Qusti, *Adv. Powder Technol.*, 2014, 25, 457–461.

33. S. Jauhar, A. Goyal, N. Lakshmi, K. Chandra and S. Singhal, *Mater. Chem. Phys.*, 2013, 139, 836-843.

34. S. Bhukal, R. Sharma, S. Mor and S. Singhal, *Superlattices Microstruct.*, 2015, 77, 134–151.

35. C. Singh, S. Bansal, V. Kumar and S. Singhal, *Ceram. Int.*, 2015, 41, 3595–3604.

36. S. Singhal, S. Jauhar, J. Singh, K. Chandra and S. Bansal, *J. Mol. Struct.*, 2012, 1012, 182–188.

37. L. X. Yang, Y. B. Xu, R. C. Jin, F. Wang, P. Yin, G. H. Li, C. P. Xu and L. B. Pan, *Ceram. Int.*, 2015, 41, 2309–2317.

38. H. L. Xin, S. Alayoglu, R. Tao, A. Genc, C. M. Wang, L. Kovarik, E. A. Stach, L.W. Wang, M. Salmeron, G. A. Somorjai and H. Zheng, *Nano lett.*, 2014, 14, 3203-3207.

39. B. D. Cullity and S. R. Stock. 2001. Elements of X-ray Diffraction, third ed. *Prentice Hall, New Jersey*.

40. C. Singh, A. Goyal and S. Singhal, *Nanoscale*, 2014, 6, 7959-7970.

41. K. Pemartin, C. Solans, J. Alvarez-Quintana and M. Sanchez-Dominguez, *Colloids Surf., A: Physicochem. Eng. Aspects*, 2014, 451, 161–171.

42. D. A. Ferrer, S. Guchhait, H. Liu, F. Ferdousi, C. Corbet, H. Xu, M. Doczy, G. Bourianoff, L. Mathew, R. Rao, S. Saha, M. Ramon, S. Ganguly, J. T. Markert, and S. K. Banerjee, *J. App. Phys.,* 2011, 110, 14316.

43. S. Singhal, J. Singh, S. K Barthwal and K. Chandra, *J. of Solid State Chem.,* 2005, 178, 3183–3189.

44. D. S. Mathew and R. S. Juang, *Chem. Eng. J.,* 2007, 129, 51–65.

45. R. Sharma, S. Bansal and S. Singhal, *RSC* adv., 2015, 5, 6006-6018.

46. S. Singhal, S. Jauhar, J. Singh, K. Chandra and S. Bansal, *J. Mol. Str.,* 2012, 1012, 182-188.

47. S. Singhal, T. Namgyal, S. Bansal and K. Chandra, *J. Electromagnetic Analysis & Applications*, 2010, 2, 376-381.

48. G. Vaidysnsthan, S. Sendhilnathan and R. Arulmurugan, *J. Magn. Magn. Mater.,* 2007, 313, 293–299.

49. S. Y. An, I. S. Kim, S. H. Son, S. Y. Song, J. W. Hahn, S. W. Hyun. C. M. Kim and C. S. Kim, *Thin Solid Films.,* 2011, 519, 8296-8298.

50. R.N. Bhowmik, V. Vasanthi and Asok Poddar, *J. Alloys Compd*., 2013, 578, 585–594.

51. R. Kaur, C. Giordano, M. Gradzielski and S. K. Mehta, *Chem. Asian J.*, 2014, 9, 189-198.

52. M. Ramesh, G. S. N. Rao, K. Samatha and B. P. Rao, *Ceram. Int*., 2015, 41, 1765–1770.

53. M. Gholinejad and A. Aminianfar, *J. Mol. Catal. A: Chem*., 2015, 397, 106–113.

54. N. Panda, A. K. Jena, S. Mohapatra and S. R. Rout, *Tetrahedron Lett*., 2011, 52, 1924–1927.

55. X. Du, J. He, J. Zhu, L. Sun and S. An, *Appl. Surf. Sci.*, 2012, 258, 2717– 2723.

56. S. U. Nandanwar and M. Chakraborty, *Chin. J. Catal.*, 2012, 33, 1532–1541.

57. S. Jana, S. K. Ghosh, S. Nath, S. Pande, S. Praharaj, S. Panigrahi, S. Basu, T. Endo and T. Pal, *Appl. Catal., A*, 2006, 313, 41–48.

58. X. Liu, Y. Yang, X. Shi and K. Li, *J. Hazard. Mater.*, 2015, 283, 267–275.

59. K. Layek, M. L. Kantam, M. Shirai, D. Nishio-Hamane, T. Sasaki and H. Maheswaran, *Green Chem.*, 2012, 14, 3164-3174.

60. A. S. Albuquerque, M. V. C. Tolentino, J. D. Ardisson, F. C. C. Moura, R. de Mendonc and W. A. A. Macedo, *Ceram. Int.*, 2012, 38, 2225–2231.

61. R. K. Sharma, Y. Monga and A. Puri, *J. Mol. Catal. A: Chem.*, 2014, 393, 84–95.

Table. 1. The values of lattice parameter, crystallite size, X-ray density, saturation magnetization, remanence, coercivity and squareness ratio for $CoM_{0.2}Fe_{1.8}O_4$ (M=Co, Ni, Cu and Zn) ferrite nanocatalysts annealed at 400 °C.

Sample	Lattice parameter (a) (A°)	crystallite size (D) (nm)	X-ray density $(d_x)(g/cm^3)$	Saturation magnetization (M_s) (emu/g)	Remanence (M_r) (emu/g)	Coercivity (H_c) (Oe)	Squareness $(S=M_r/M_s)$
$Co_{1.2}Fe_{1.8}O_4$	8.392	17.33	5.287	36.6	14.0	1288	0.38
$CoNi_{0.2}Fe_{1.8}O_4$	8.379	15.59	5.310	36.4	14.5	1351	0.40
$CoCu_{0.2}Fe_{1.8}O_4$	8.373	14.85	5.344	40.3	12	533	0.30
$CoZn_{0.2}Fe_{1.8}O_4$	8.389	14.83	5.322	39.2	16	1495	0.41
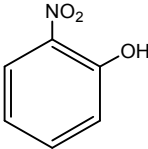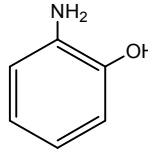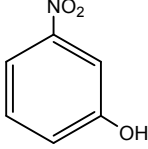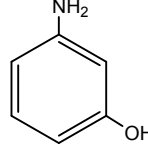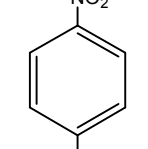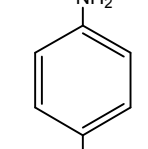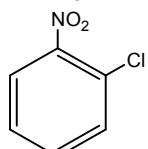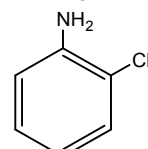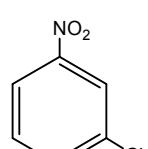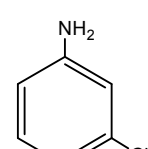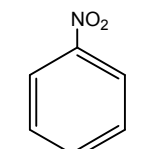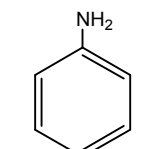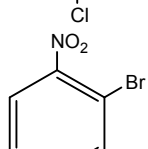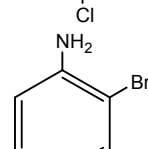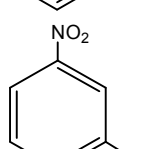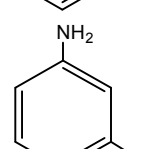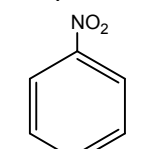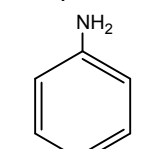
Table. 2. Completion time values for the reduction of nitrophenols in the presence of varying amount of CoCu$_{0.2}$Fe$_{1.8}$O$_4$ nanocatalyst annealed at 400 °C.
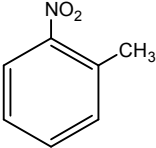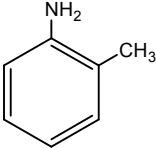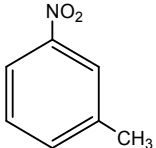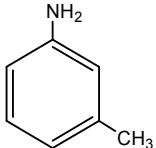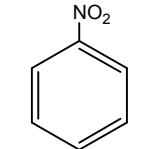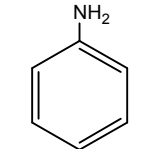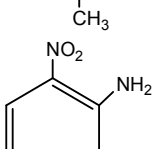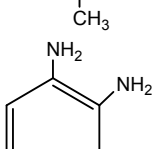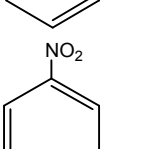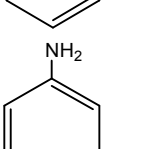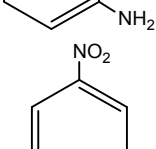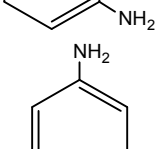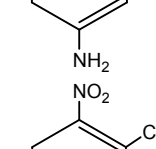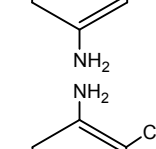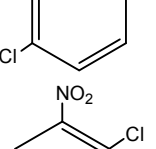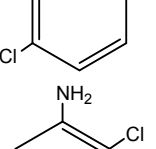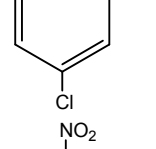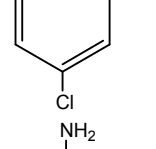
Catalyst mole %	2-nitrophenol	3-nitrophenol	4-nitrophenol
	Completion time (minutes)		
2 mole %	8.0	15.0	13.0
5 mole %	4.0	9.0	8.0
10 mole %	3.0	5.5	5.0
20 mole %	2.0	2.5	2.5
30 mole %	1.0	2.0	1.5
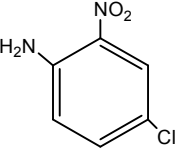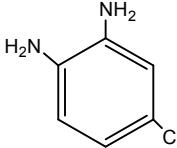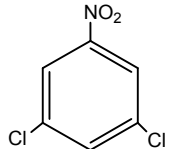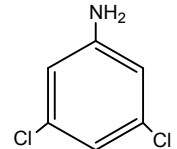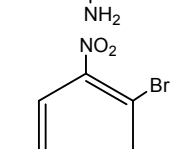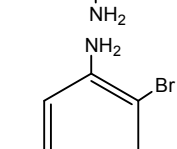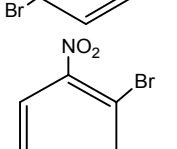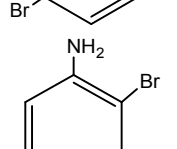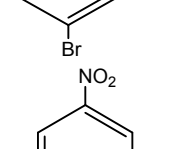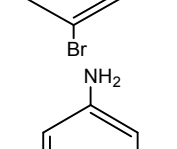
Table 3. Apparent rate constant values for the reduction of nitrophenols in the presence of varying amount of $CoCu_{0.2}Fe_{1.8}O_4$ nanocatalyst annealed at 400 °C.

Amount of $CoCu_{0.2}Fe_{1.8}O_4$	2-nitrophenol	3-nitrophenol	4-nitrophenol
		Apparent rate Constant (-K_{app})	
2 mole %	0.27	0.11	0.25
5 mole %	0.66	0.26	0.34
10 mole %	1.07	0.45	0.57
20 mole %	2.78	0.95	0.98
30 mole %	3.12	1.08	2.10

Table. 4. **The values of time taken for complete conversion, conversion %, selectivity % and TOF (turn over frequency) for all the nitroarenes in the presence of 10 mole % of CoCu$_{0.2}$Fe$_{1.8}$O$_4$ ferrite nanaocatalyst annealed at 400 °C.**

Serial no.	substrate	product	Time (min)	Conversion %/ Selectivity %	TOF (mole/mole/hour)
1.	(2-nitrophenol)	(2-aminophenol)	3	100/100	200.0
2.	(3-nitrophenol)	(3-aminophenol)	5.5	100/100	109.0
3.	(4-nitrophenol)	(4-aminophenol)	5	100/100	120.0
4.	(2-nitrochlorobenzene)	(2-chloroaniline)	21	100/100	28.6
5.	(3-nitrochlorobenzene)	(3-chloroaniline)	75	100/100	8.0
6.	(4-nitrochlorobenzene)	(4-chloroaniline)	28	100/100	21.4
7.	(2-nitrobromobenzene)	(2-bromoaniline)	21	100/67	19.2
8.	(3-nitrobromobenzene)	(3-bromoaniline)	55	100/86	9.4
9.	(4-nitrobromobenzene)	(4-bromoaniline)	25	100/63	15.1

No.				
10.	NO$_2$ / CH$_3$ — NH$_2$ / CH$_3$	40	100/100	15.0
11.	NO$_2$ / CH$_3$ — NH$_2$ / CH$_3$	48	100/100	12.5
12.	NO$_2$ / CH$_3$ — NH$_2$ / CH$_3$	25	100/100	24.0
13.	NO$_2$ / NH$_2$ — NH$_2$ / NH$_2$	15	100/100	40.0
14.	NO$_2$ / NH$_2$ — NH$_2$ / NH$_2$	18	100/100	34.0
15.	NO$_2$ / NH$_2$ — NH$_2$ / NH$_2$	24	100/100	25.0
16.	NO$_2$ / Cl / Cl — NH$_2$ / Cl / Cl	12	100/100	50.0
17.	NO$_2$ / Cl / Cl — NH$_2$ / Cl / Cl	15	100/100	40.0
18.	NO$_2$ / Cl / NH$_2$ — NH$_2$ / Cl / NH$_2$	28	100/100	21.5

19.			5	100/100	120.0
20.			10	100/100	60.0
21.			15	100/70	28.0
22.			35	100/88	15.1
23.			2	100/68	204.0
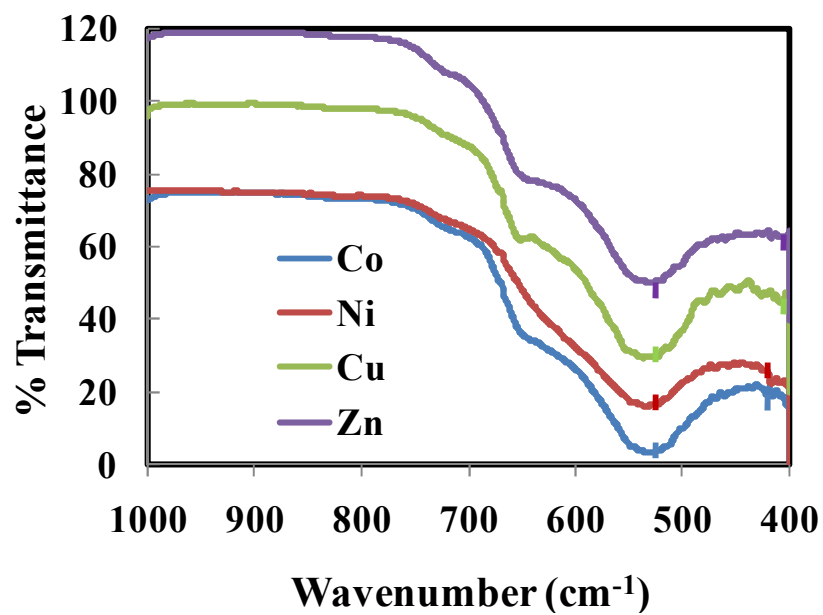
Fig. 1. The FT-IR spectra for CoM$_{0.2}$Fe$_{1.8}$O$_4$ (M=Co, Ni, Cu and Zn) ferrite nanocatalysts annealed at 400 °C.
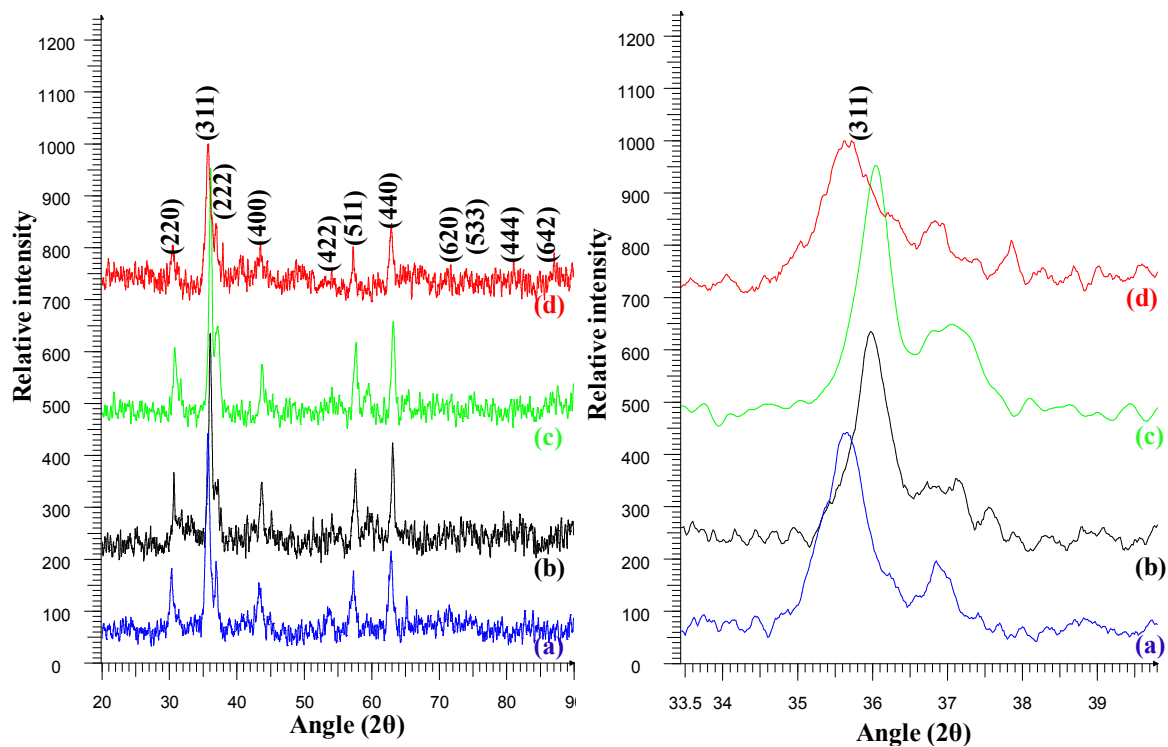
Fig. 2. XRD patterns for $CoM_{0.2}Fe_{1.8}O_4$ (M= Co (a), Ni (b), Cu (c) and Zn (d)) ferrite nanocatalysts annealed at 400 °C and Enlarged (3 1 1) peak.
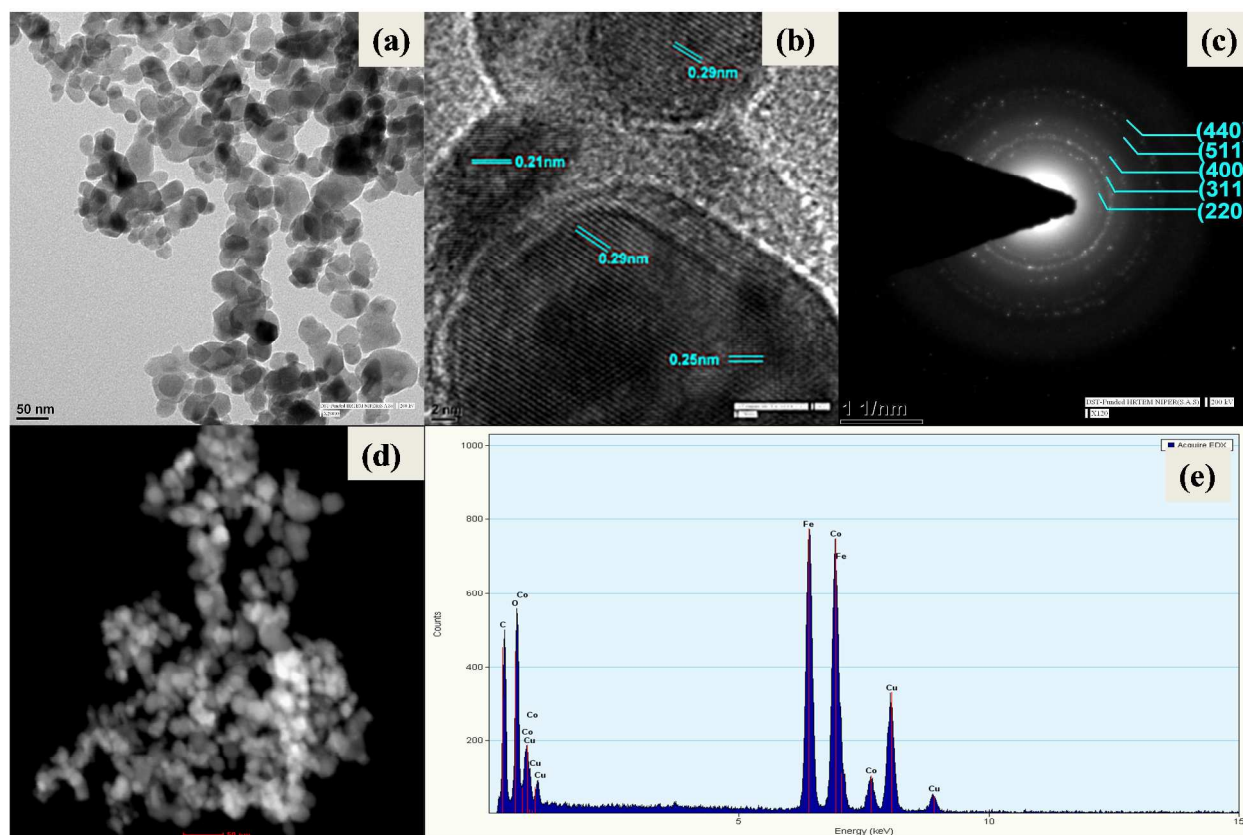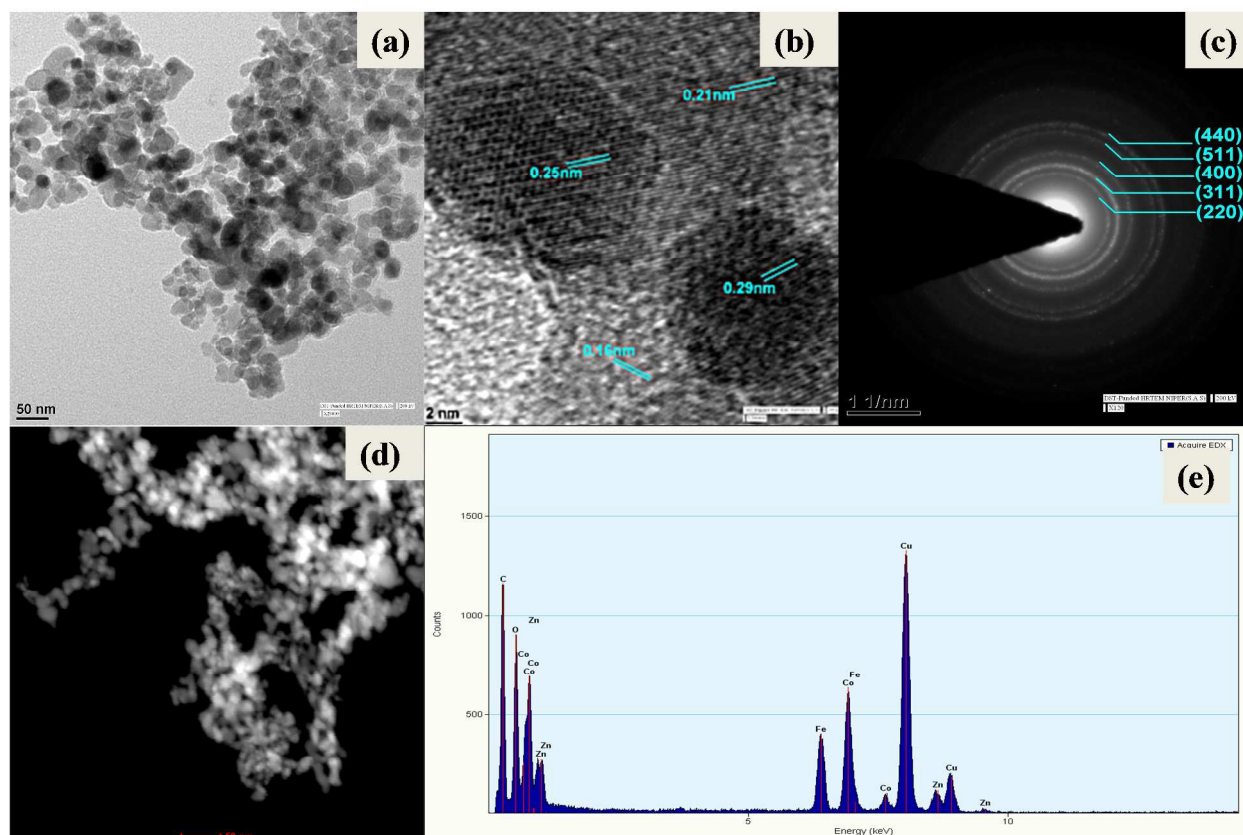
Fig. 3. TEM images of the Co$_{1.2}$Fe$_{1.8}$O$_4$ ferrite nanocatalyst annealed at 400 °C (a) at low resolution (b) at high resolution (C) SAED pattern (d) STEM image and (e) EDX spectra.
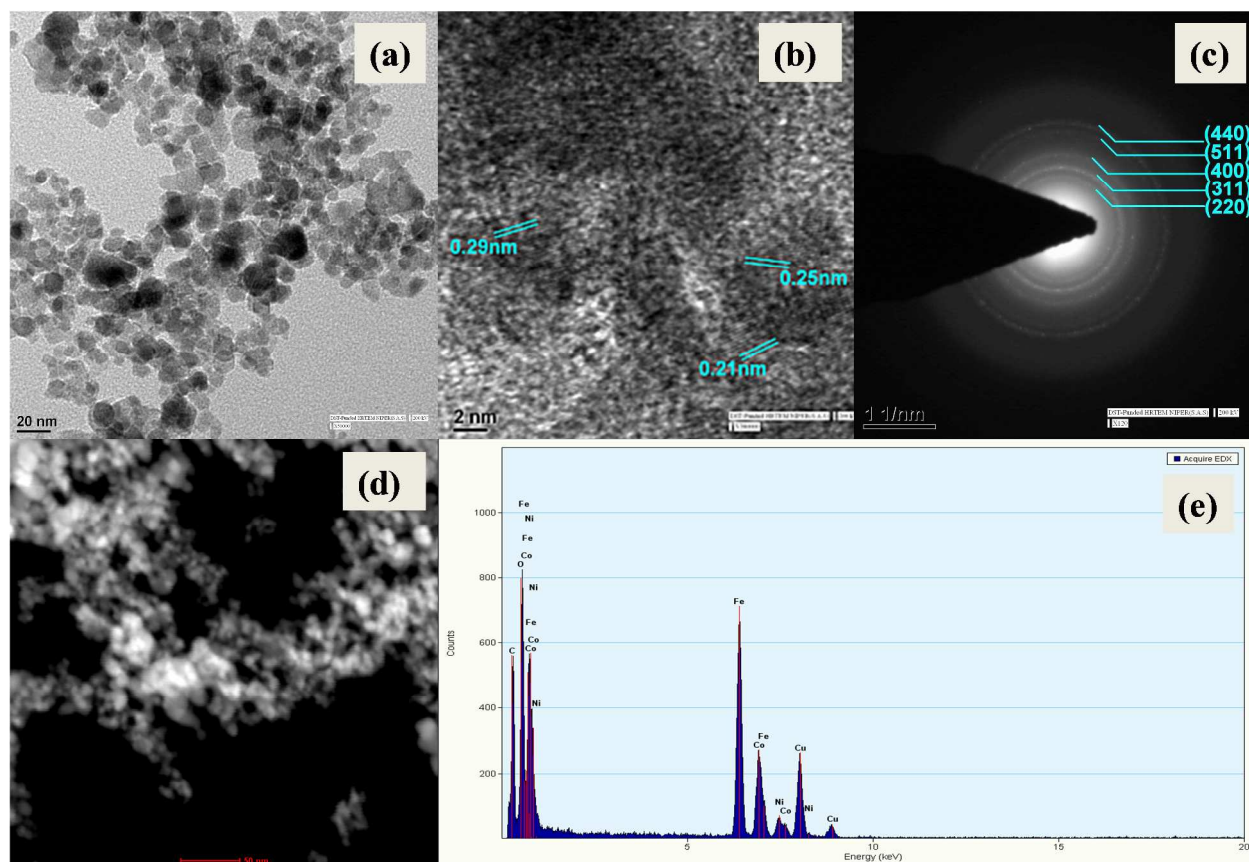
Fig. 4. TEM images of the CoNi$_{0.2}$Fe$_{1.8}$O$_4$ ferrite nanocatalyst annealed at 400 °C (a) at low resolution (b) at high resolution (C) SAED pattern (d) STEM image and (e) EDX spectra.
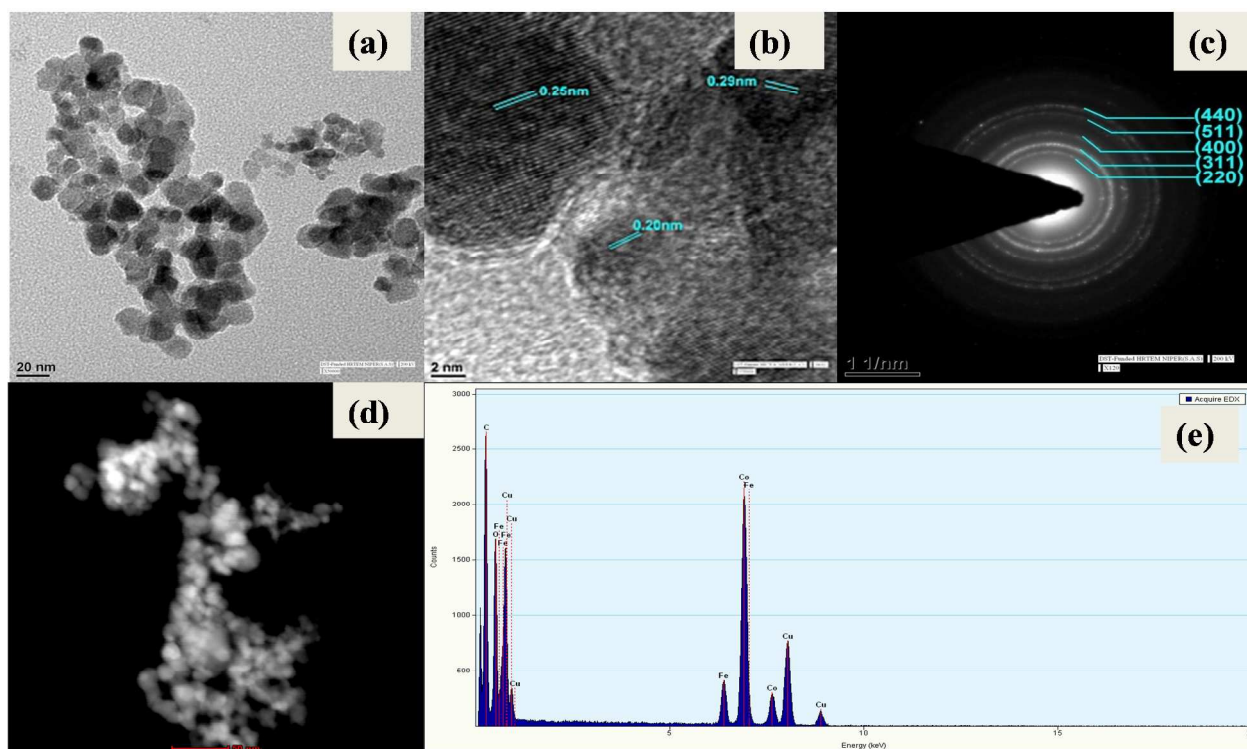
Fig. 5. TEM images of the CoCu$_{0.2}$Fe$_{1.8}$O$_4$ ferrite nanocatalyst annealed at 400 °C (a) at low resolution (b) at high resolution (C) SAED pattern (d) STEM image and (e) EDX spectra.

Fig. 6. TEM images of the CoZn$_{0.2}$Fe$_{1.8}$O$_4$ ferrite nanocatalyst annealed at 400 °C (a) at low resolution (b) at high resolution (C) SAED pattern (d) STEM image and (e) EDX spectra.
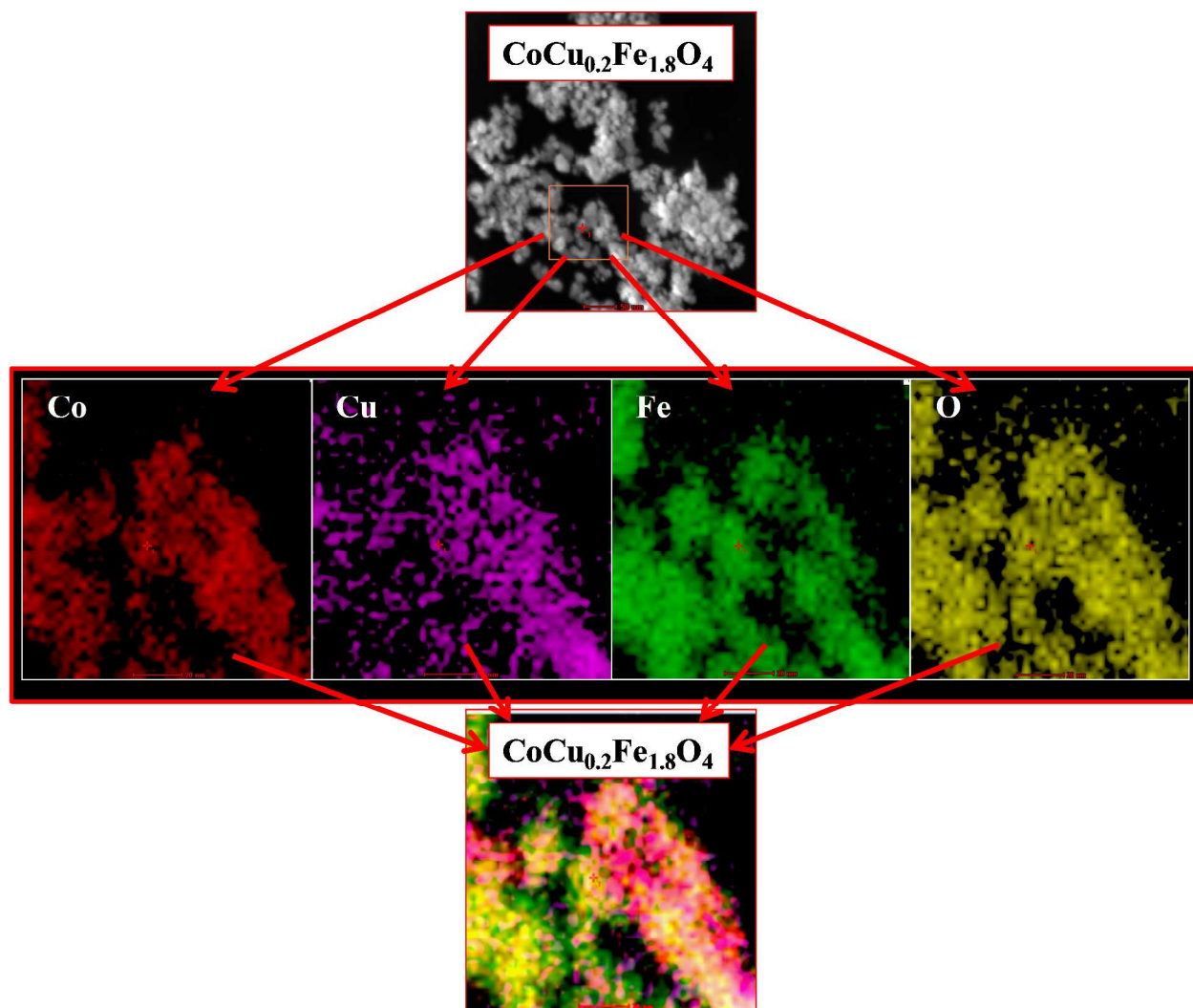
Fig. 7. Typical STEM-EDX mapping for CoCu$_{0.2}$Fe$_{1.8}$O$_4$ ferrite nanocatalyst annealed at 400 °C.
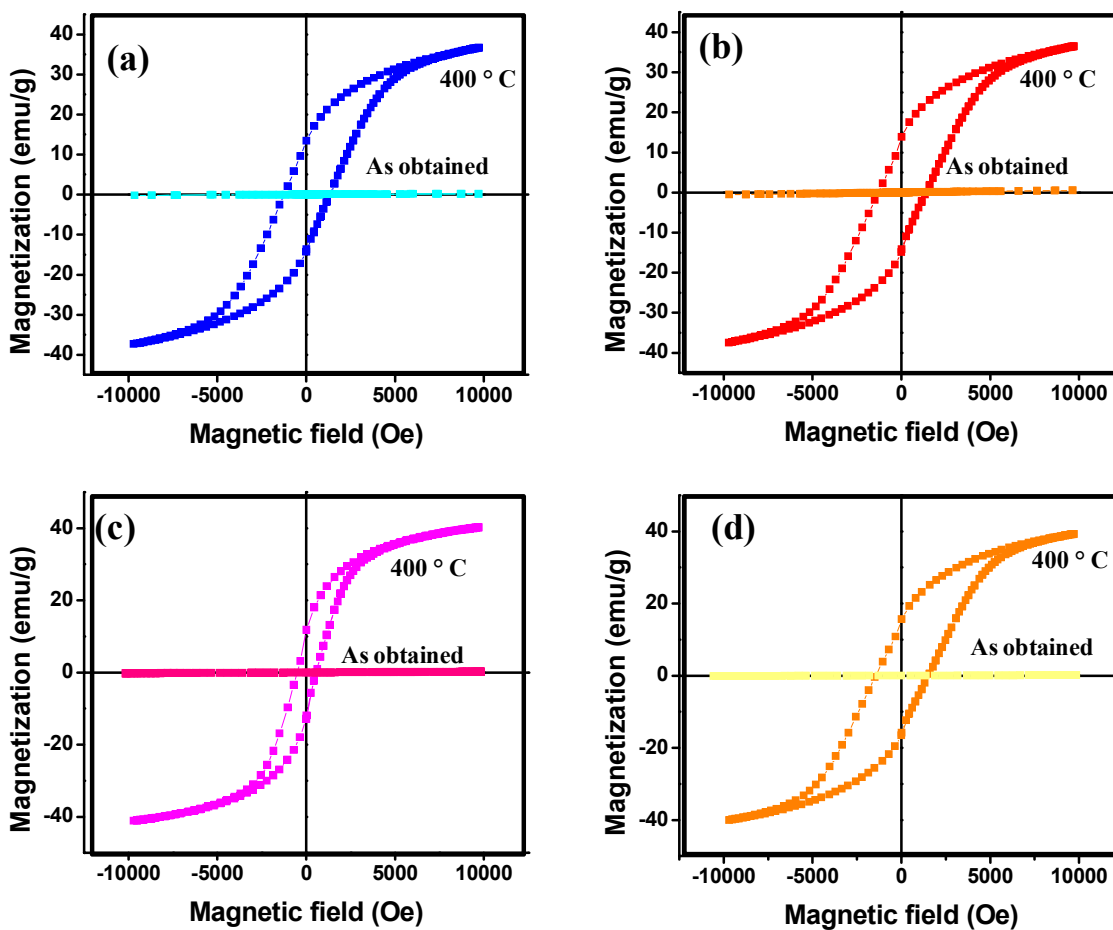
Fig.8 Room temperature hysteresis loops for CoM$_{0.2}$Fe$_{1.8}$O$_4$ (M= Co (a), Ni (b), Cu (c), Zn (d)) ferrite nanocatalysts as obtained and annealed at 400 °C.
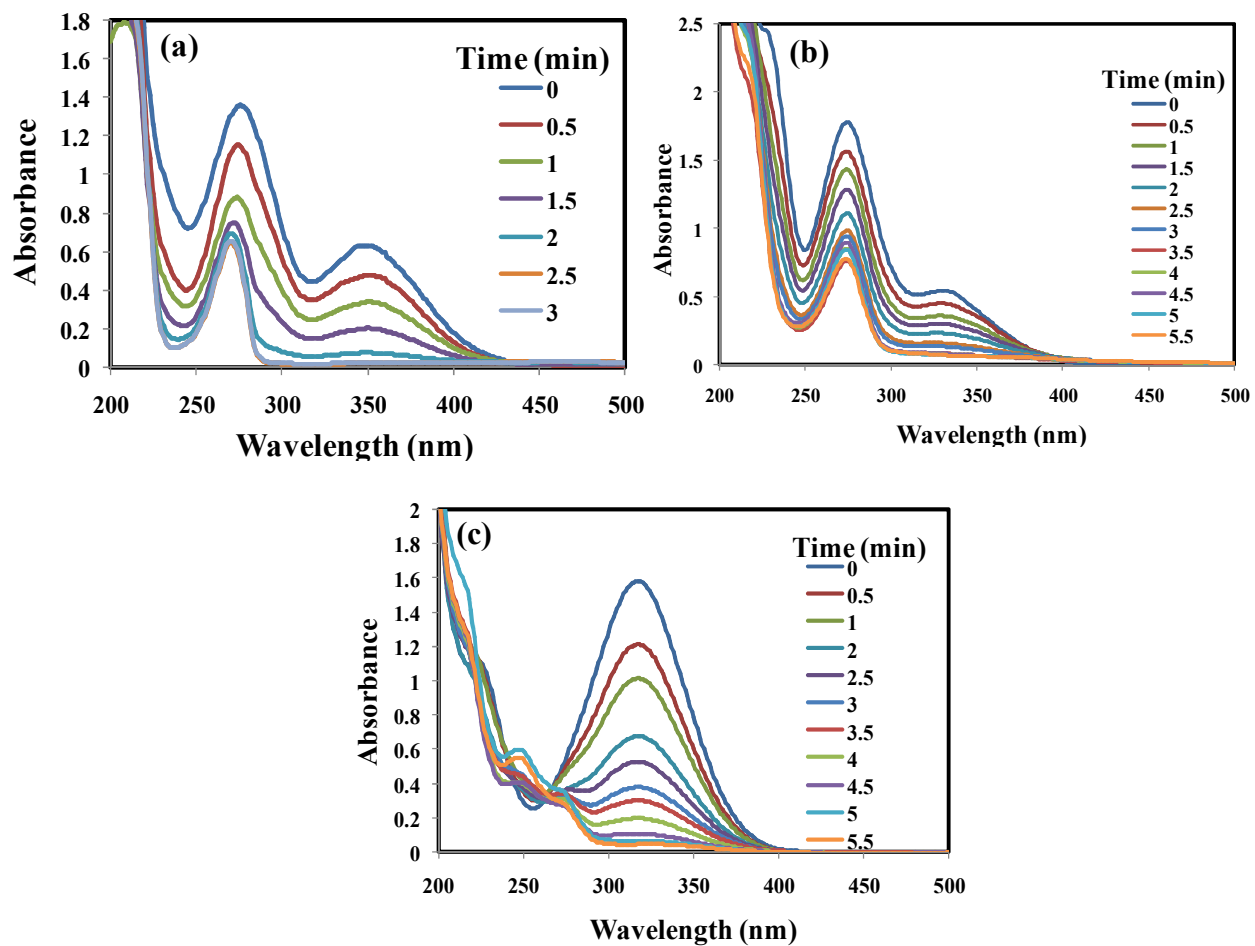
Fig. 9. UV-Visible spectra for the reduction of (a) 2-nitrophenol, (b) 3-nitrophenol and (c) 4-nitrophenol in the presence of 10 mole % of $CoCu_{0.2}Fe_{1.8}O_4$ ferrite nanocatalyst annealed at 400 °C.
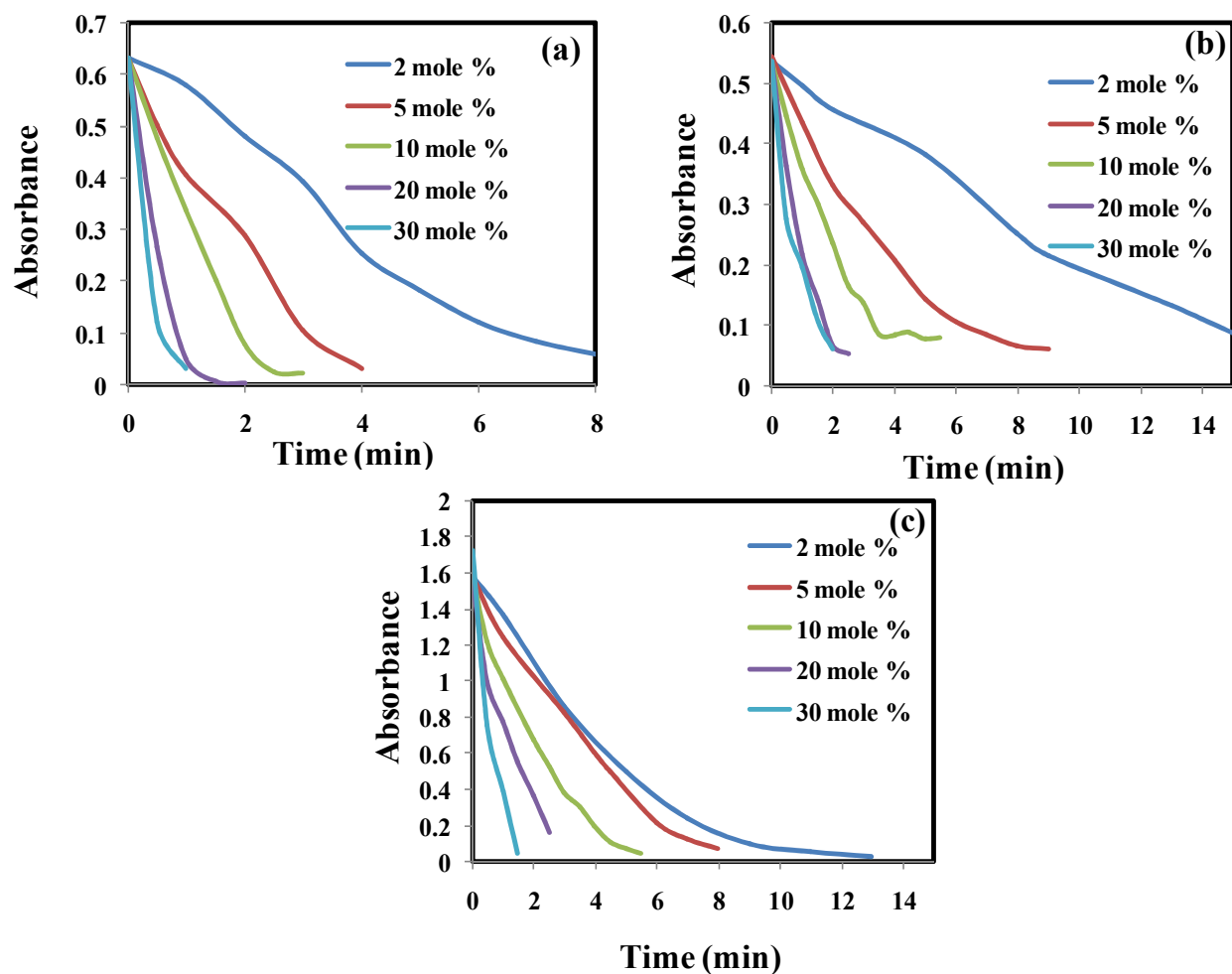
Fig. 10. The Absorbance Vs. Time curves for the reduction of (a) 2-nitrophenol, (b) 3-nitrophenol and (c) 4-nitrophenol in the presence of varying amounts of $CoCu_{0.2}Fe_{1.8}O_4$ ferrite nanocatalyst annealed at 400 °C.
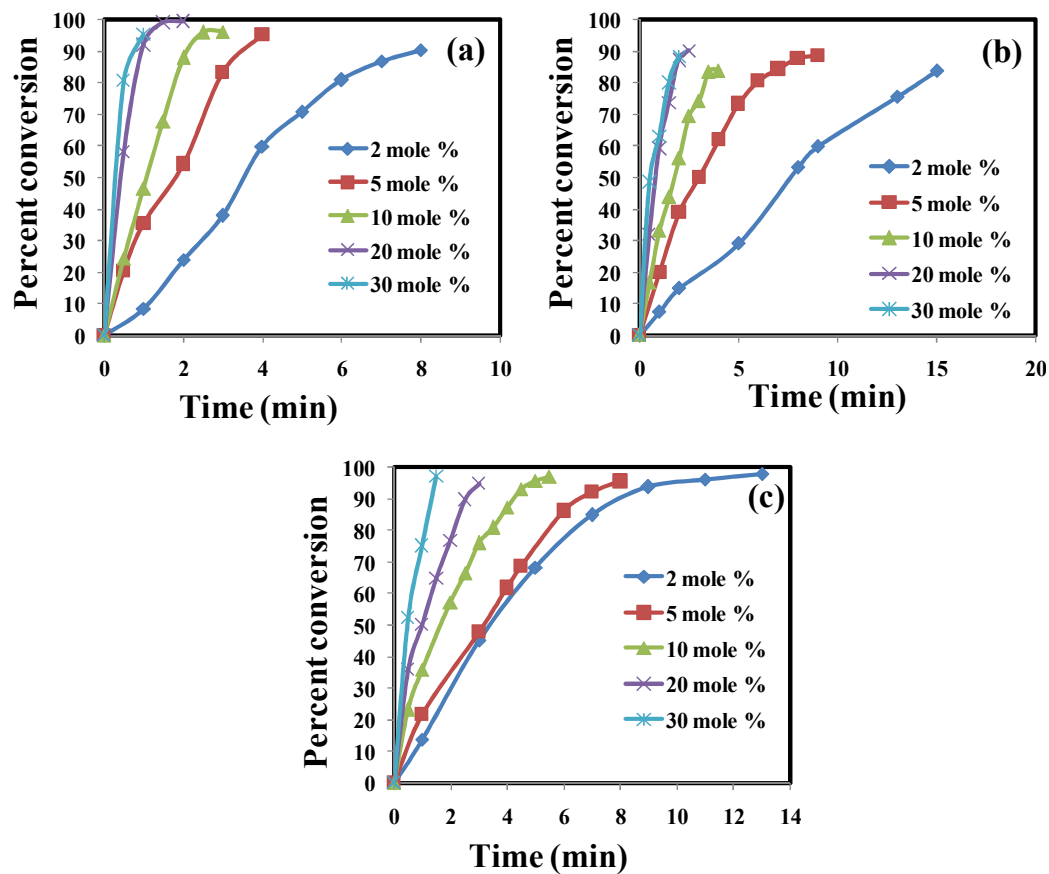
Fig. 11. The Percent conversion Vs. Time curves for the reduction of (a) 2-nitrophenol, (b) 3-nitrophenol and (c) 4-nitrophenol in the presence of varying amounts of $CoCu_{0.2}Fe_{1.8}O_4$ ferrite nanocatalyst annealed at 400 °C.
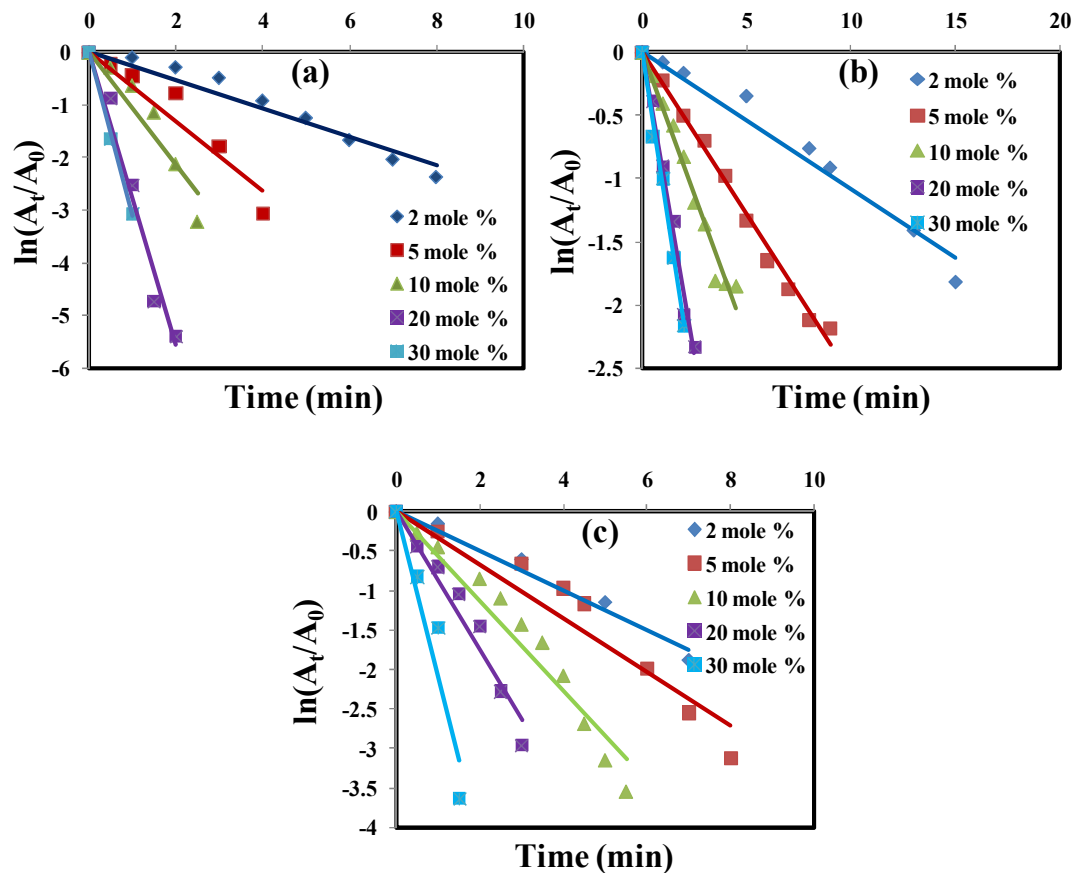
Fig. 12. The Plots of ln(A$_t$/A$_o$) vs time (t) for the reduction of (a) 2-nitrophenol, (b) 3-nitrophenol and (c) 4-nitrophenol in the presence of varying amounts of CoCu$_{0.2}$Fe$_{1.8}$O$_4$ ferrite nanocatalyst annealed at 400 °C.
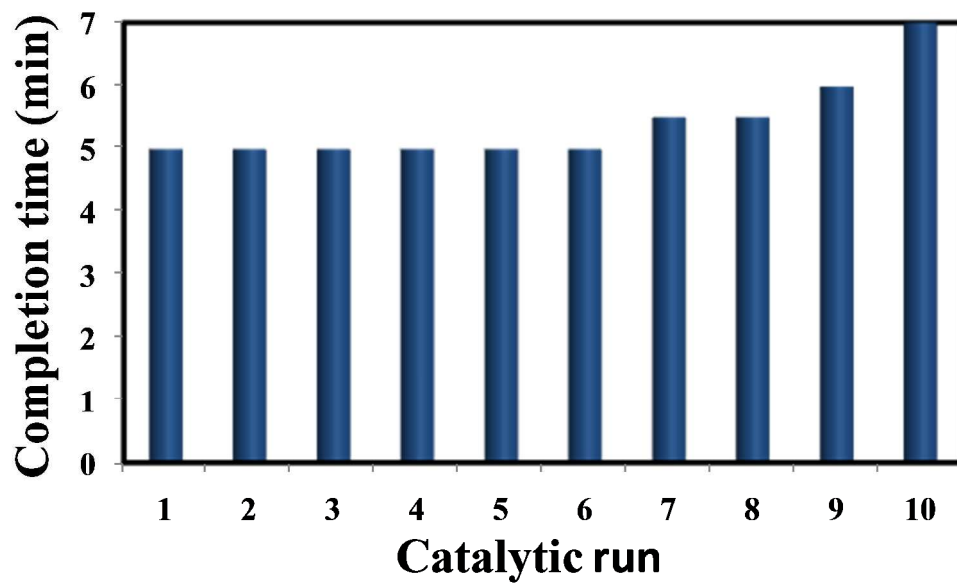
Fig. 13. The variation of completion time for successive catalytic runs.